Biophysical Journal
Article

Biophysical Society

Protein Diffusion on Charged Biopolymers: DNA versus Microtubule

Lavi S. Bigman[1] and Yaakov Levy[1,*]
[1]Department of Structural Biology, Weizmann Institute of Science, Rehovot, Israel

ABSTRACT Protein diffusion in lower-dimensional spaces is used for various cellular functions. For example, sliding on DNA is essential for proteins searching for their target sites, and protein diffusion on microtubules is important for proper cell division and neuronal development. On the one hand, these linear diffusion processes are mediated by long-range electrostatic interactions between positively charged proteins and negatively charged biopolymers and have similar characteristic diffusion coefficients. On the other hand, DNA and microtubules have different structural properties. Here, using computational approaches, we studied the mechanism of protein diffusion along DNA and microtubules by exploring the diffusion of both protein types on both biopolymers. We found that DNA-binding and microtubule-binding proteins can diffuse on each other's substrates; however, the adopted diffusion mechanism depends on the molecular properties of the diffusing proteins and the biopolymers. On the protein side, only DNA-binding proteins can perform rotation-coupled diffusion along DNA, with this being due to their higher net charge and its spatial organization at the DNA recognition helix. By contrast, the lower net charge on microtubule-binding proteins enables them to diffuse more quickly than DNA-binding proteins on both biopolymers. On the biopolymer side, microtubules possess intrinsically disordered, negatively charged C-terminal tails that interact with microtubule-binding proteins, thus supporting their diffusion. Thus, although both DNA-binding and microtubule-binding proteins can diffuse on the negatively charged biopolymers, the unique molecular features of the biopolymers and of their natural substrates are essential for function.

SIGNIFICANCE Several cellular functions are governed by linear diffusion of proteins on biopolymers. For example, diffusion is essential for DNA scanning while proteins search for their cognate site or protein localization to specific microtubule regions. Because both DNA and microtubule are negatively charged and the corresponding measured diffusion coefficients are similar, it is tempting to classify these two types of diffusion as sharing similar driving forces. Here, we investigate what is needed for a protein to linearly diffuse on a charged biopolymer and what distinguishes diffusion on DNA from diffusion on a microtubule. Quantifying the diffusion mechanisms may not only shed light on their molecular determinants but also formulate principles for manipulating protein diffusion in a low-dimensional space.

INTRODUCTION

Diffusion is a common transport mechanism in the cell, particularly when it takes place in lower-dimensionality spaces, such as proteins diffusing along one-dimensional (1D) biological polymers or on two-dimensional surfaces. Examples for 1D diffusion are the dynamics of proteins along DNA or along microtubules (MTs), whereas two-dimensional diffusion describes the motion of proteins along membranes. These diffusion processes are essential for proper cellular function. Although each diffusion mechanism potentially has unique characteristics, they share some common features, such as the role of long-range electrostatic forces in mediating diffusion.

MTs, which are an essential component of the eukaryotic cytoskeleton, provide mechanical support to the cell and serve as "highways" for intracellular trafficking. In addition to the well-known ATPase-mediated unidirectional active transport of cargo by motor proteins from the kinesin and dynein superfamilies (1–3), many MT-binding proteins (MBPs) diffuse along the MT lattice to reach various target sites (4). For instance, EB1 (5), the Dam1 complex (6), XMAP215 (7), kinesin 13 (mitotic centromere-associated kinesin) (8), and the Ndc80 complex (9) use diffusion to reach the plus end of MTs, where they are involved in tight regulation of MT length, which is crucial for cell division and neuronal development. By contrast, both PRC1 (5) (which cross-links two antiparallel MTs to form spindle

Submitted February 26, 2020, and accepted for publication May 12, 2020.
*Correspondence: koby.levy@weizmann.ac.il
Editor: Anatoly Kolomeisky.
https://doi.org/10.1016/j.bpj.2020.05.004
© 2020 Biophysical Society.

midzones at anaphase (10)) and the intrinsically disordered protein Tau (11) (which increases the stability of neuronal MTs) diffuse along the MT lattice, although they do not need to reach a specific end. Interestingly, some motor proteins combine diffusional and directed motility to diffuse in a biased manner along the MT lattice (12–15) or to sidestep across MT protofilaments (16,17), which may provide them with a mechanism to overcome roadblocks on a crowded MT lattice.

Protein diffusion along DNA constitutes another important example of protein diffusion along charged biopolymers. DNA-binding proteins (DBPs) perform various biological tasks, such as controlling transcription and repairing damaged DNA, all of which involve scanning the DNA by linear diffusion before specific recognition at the functional site. Theoretical and experimental perspectives have attributed the remarkable efficiency and specificity of protein-DNA recognition to the 1D diffusion of proteins on DNA (18–20). Furthermore, diffusion along DNA has been observed experimentally for various DBPs, such as RNA polymerase (21), the *lac* repressor (22), p53 (23–25), and Egr-1 (26,27) transcription factors, and for mismatch repair complexes (28), and its mechanisms have been further quantified by theoretical and computational studies (29–41).

Protein diffusion along DNA and MTs share many similarities. First, the diffusion coefficients for DBPs and MBPs are similar and span four orders of magnitude from 0.001 to 1 $\mu m^2/s$ (Fig. 1). Interestingly, the diffusion of proteins on membranes, another charged biological surface, has been reported for several systems (42–45), and diffusion coefficients were found to be in the range of 0.4–2.5 $\mu m^2/s$, which is the same order of magnitude as for DBPs and MBPs.

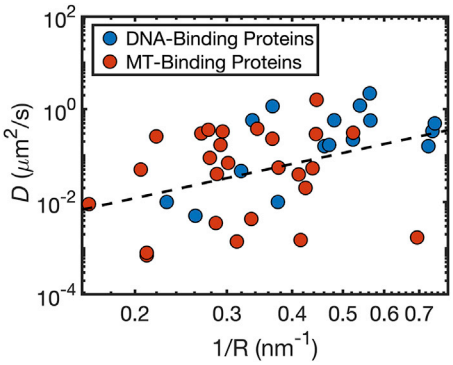

FIGURE 1 A survey of experimentally measured protein diffusion coefficients on DNA and MT molecules. The diffusion coefficients, D, of 16 DNA-binding proteins (DBPs; *blue circles*) and 26 MT-binding proteins (MBPs; *red circles*) are shown as a function of the reciprocal radius (R) of each protein. The diffusion coefficients of both types of proteins span approximately four orders of magnitude and depend linearly on $1/R$, consistently with the Stokes-Einstein diffusion relation ($D = K_B T/6\pi\eta R$), as indicated by the dashed black line, which is the best linear fit to all the data points in this figure (slope = 2.4, R = 0.41). The protein radius, R, was estimated from the protein chain length (73) because the three-dimensional structures of many of these proteins have not been resolved. The full data set is summarized in Table S1. To see this figure in color, go online.

The similarity between DBP-DNA and MBP-MT interactions is also reflected in their corresponding binding affinities. The affinity of MBPs and DBPs to their respective polymers covers approximately three orders of magnitude, with dissociation constants ranging from the micromolar to low nanomolar ranges (5,27,46–49). The affinity of DBPs may depend on whether they bind to a nonspecific or specific DNA sequence (27), whereas the affinity of MBPs may depend not only on the binding site but also on the nucleotide state of the MT (49) or nucleotide state of the MBP itself (for motor proteins) (47).

The similar range of diffusion coefficients for protein diffusion on MTs and on DNA can be attributed to the similarity of their driving forces because the two processes share similar electrostatic characteristics: the surface of both MT and DNA are negatively charged, and their corresponding diffusing proteins are positively charged. Moreover, because of their long-range nature, electrostatic interactions were suggested to play a central role in the mechanism of various diffusion processes along periodic substrates (39,50–52). Particularly, the role of electrostatic forces in the protein diffusion emerges from computational and experimental studies, illustrating for both DNA (39,53) and MTs (5,11) the sensitivity of their diffusion coefficient to salt concentration.

Although the surfaces of both MTs and DNA are negatively charged, the similar protein diffusion coefficient values are somewhat surprising given the structural differences between the two polymers. First, MTs are much larger than DNA: the diameter of MTs is ~25 nm, which is an order of magnitude larger than the ~2-nm-wide DNA. In addition, DNA and MT differ in their periodicity, which affects the elementary step size of diffusion along their main axis. The step size relevant for diffusion along DNA is on the order of a single basepair, i.e., ~0.5 nm, whereas the step size for diffusion along MTs is on the order of a tubulin monomer or dimer, i.e., 4–8 nm (54,55). Moreover, the double helix of DNA is characterized by two grooves that do not exist in MTs. On the other hand, MTs are decorated with intrinsically disordered, negatively charged C-terminal tails that are known to regulate the interactions of MTs with several partner proteins (56–60). Hence, it is possible that these structural differences will be reflected in the diffusion mechanisms of proteins on DNA and MTs.

Although there have been extensive independent studies of each biopolymer and its binding proteins, no direct comparison has been made between the diffusion of proteins on DNA and MTs despite the potential of such a comparison to elucidate the unique features of MTs, DNA, and their binding proteins. In this study, we explored the difference between the two linear diffusion processes by asking whether DBPs can diffuse on MTs or whether MBPs can diffuse on DNA in a similar fashion to the diffusion

performed on their functional biopolymer substrates. Specifically, we applied coarse-grained (CG) molecular dynamics (MD) simulations complemented by bioinformatic analysis to directly compare the molecular details of protein diffusion on DNA and MTs. For this purpose, we chose three DBPs (Skn1, SAP1, and the engrailed homeodomain (HD)) and three MBPs (EB1, PRC1, and Tau) and studied their diffusion on both DNA and MTs. We found that MBPs diffuse faster than DBPs on both DNA and MTs, mainly because MBPs are less positively charged than DBPs. In addition, we demonstrated that the major groove of the DNA and the disordered tubulin tails on MTs are key regulators of protein diffusion on charged biological polymers. These observations were complemented by a bioinformatic analysis, which supports the generalizability of our conclusions.

METHODS

CG-MD simulations

The dynamics of protein diffusion along MTs and DNA was studied using CG-MD simulations that enable the investigation of long timescale processes that are challenging for high-resolution models. Each residue was represented by a single bead at the position of its Cα-atom. The DNA was modeled with three beads per nucleotide, representing the phosphate, sugar, and base (61).

The force field applied in our simulations used a native-topology-based model that includes a Lennard-Jones potential to reward native contacts and a repulsive potential to penalize non-native contacts (62–64). Electrostatic interactions between charged residues (the bead representing the DNA phosphate groups that bear a negative charge in our model) were modeled using the Debye-Hückel potential (65). The explicit form of the force field is the following:

$$
\begin{aligned}
V(\Gamma,\Gamma_0) = &\sum_{bonds} K_{bonds}\left(b_{ij}-b_{ij}^0\right) + \sum_{angles} K_{angles}\left(\theta_{ijk}-\theta_{ijk}^0\right)\\
&+ \sum_{dihedrals} K_{dihedrals}\left(\left[1-\cos\left(\varphi_{ijkl}-\varphi_{ijkl}^0\right)\right]\right.\\
&\left.+\frac{1}{2}\left[1-\cos\left(3\left(\varphi_{ijkl}-\varphi_{ijkl}^0\right)\right)\right]\right)\\
&+ \sum_{i\neq j} K_{contacts}\left[5\left(\frac{A_{ij}}{r_{ij}}\right)^{12}-6\left(\frac{A_{ij}}{r_{ij}}\right)^{10}\right]\\
&+ \sum_{i\neq j} K_{repulsions}\left(\frac{C_{ij}}{r_{ij}}\right)^{12}\\
&+ \sum_{i\neq j} K_{electrostatics} B(\kappa) q_i q_j \frac{e^{-\kappa r}}{\varepsilon_r r_{ij}},
\end{aligned}
$$

where $K_{bonds} = 100$ kcal mol^{-1} Å^{-2}; $K_{angles} = 20$ kcal mol^{-1}; and $K_{dihedrals}$, $K_{contacts}$, and $K_{repulsion}$ are each valued at 1 kcal mol^{-1}. The term b_{ij} is the distance (in angstroms) between bonded beads *i-j*, θ_{ijk} is the angle (in radians) between sequentially bonded beads *i-j-k*, φ_{ijkl} is the dihedral angle (in radians) between sequentially bonded backbone beads *i-j-k-l*, and r_{ij} is the distance (in angstroms) between beads *i-j* in a given conformation along the trajectory. A_{ij} is the distance (in angstroms) between beads *i-j* that are in contact with each other in the experimentally determined structure. The parameters denoted with the superscript 0 (x^0) represent the minima of the various potential energy terms that were assigned according to the atomic coordinates of the structures. C_{ij} is the sum of radii for any two beads not forming a native contact; the repulsion radius of the backbone bead is 2.0 Å. The last term in the force field is the Debye-Hückel potential, where $K_{electrostatics} = 332$ kcal Å mol^{-1} e^{-2}, $q_{i/j}$ is the sign of the charged residue, ε_r is the dielectric constant, κ is the screening factor, B(κ) is the salt-dependent coefficient, and r_{ij} is the distance (in angstroms) between charged residues *i* and *j*. We note that, because of the CG representation of the systems, the effective salt concentration may correspond to a value higher (by a factor of ~3) than for an atomistic representation. More details regarding the Debye-Hückel potential can be found in (65).

To reduce computational time, electrostatic interactions between the diffusing proteins and the charged residues of both α- and β-tubulins located at the interior of the MTs were eliminated. This elimination did not affect the properties of the MT surface, which is the side relevant to the diffusion process because the distance between the MT lumen and surface is ~40 Å.

The beads of the structured part of the MT (referred to herein as the "MT body") were kept fixed in our simulations, whereas the MT tails were flexible. Avoiding internal flexibility for the folded domains of the MT body is a reasonable assumption given the rigidity of MT structures. This approach also avoids deformation of the MT slice used in our summations. Furthermore, the internal dynamics of the tubulin monomers is not expected to contribute to diffusion on MT. The flexibility of the disordered MT tails was controlled by their bonds and dihedral angles.

The dynamics of protein diffusion along MTs and DNA was simulated using the Langevin equation. The simulation temperature was set to 0.4 (reduced units), which is lower than the folding temperatures of EB1, PRC1, SAP1, HD, and Skn1. The Tau protein is intrinsically disordered and was simulated at the same temperature for consistency. The dielectric constant was 70, and the salt concentration was 0.02 M unless stated otherwise.

Diffusion on DNA

The DNA and diffusing protein were confined in a box of dimensions 300 × 300 × 300 Å, and the longitudinal direction of the DNA was aligned along the *z* axis. We performed 10 simulations consisting of 10^7 MD steps. The DNA was modeled as a linear double-stranded B-DNA molecule with a length of 100 basepairs. The diffusing DBPs were HD (66) (Protein Data Bank, PDB: 1hdd), SAP1 (67) (PDB: 1bc8), and Skn1 (68) (PDB: 1skn).

Diffusion on MTs

To study the diffusion of proteins along MTs, we constructed an MT lattice consisting of four protofilaments, each consisting of three heterodimeric tubulin molecules (i.e., the lattice included 6 × 4 monomeric tubulin proteins). The coordinates of the MT lattice were based on the structure of a single isoform neuronal human MT (PDB: 5JCO) (69). The disordered tails (residues 438–451 of α-tubulin and 427–450 of β-tubulin) were added as linear chains to the C-terminal of each tubulin monomer. A more realistic conformation of the tails was obtained by the simulations. We chose to study MT-bearing tails of isoform α1A and β3, which comprise 14 and 24 residues, respectively. The sequences of the tubulin tails were DSVEGEGEEEGEEY for α-tubulin (isoform α1A, net charge of −8) and DATAEEEGEMYEDDEEESEAQGPK for β-tubulin (isoform β3, net charge of −11). The diffusing MBPs were domains of EB1 (70) (PDB: 1pa7), PRC1 (71) (PDB: 5kmg), and Tau (72) (PDB: 6cvj). The MT and diffusing proteins were confined in a box of dimensions 350 × 400 × 330 Å, and the longitudinal direction of the MT was aligned along the *y* axis. Because the scale of diffusion length along an MT lattice is longer than that along a DNA molecule, we performed 50 simulations consisting of 2 × 10^7 essential MD steps to achieve sufficient sampling. Trajectory frames were saved every 1000 steps. Periodic boundary conditions were not used in our model.

Calculation of diffusion coefficients

The trajectories from the CG simulations were analyzed using in-house scripts. The mean-square displacements of the proteins' centers of mass (COMs) were calculated using the equation as follows:

$$MSD(\tau) = \sum_{i=t_0}^{t-\tau} \frac{(r_{i+\tau} - r_i)^2}{t-\tau} = 2dD\tau,$$

where r is the position of the protein COM, t is the number of time steps measured, and τ is the measurement window ranging from t_0 to t. The slope of the mean-square displacement is $2dD$, where d is the dimensionality of diffusion and D is the diffusion coefficient, which was calculated between time frames 1500 and 3000 for diffusion on MTs because shorter timescales do not capture the slow diffusion process. For diffusion along DNA, D was calculated between time frames 1 and 200. We calculated diffusion along MT protofilaments or the DNA axis; hence, $d = 1$ in all the calculations used in this study.

Calculation of rotation-translation coupling

The angle of rotation between the diffusing protein and the DNA was calculated by the following:

$$\theta = \tan^{-1}\left(\frac{y}{x}\right),$$

where y and x are the corresponding coordinates of the protein COM around the DNA that was aligned along the z axis.

Data set of DBPs and MBPs with experimentally measured diffusion coefficients

The diffusion data for DBPs and MBPs were collected from experimental studies (see Table S1 and references therein). Because many proteins in our data set do not have a resolved three-dimensional structure, we estimated the radius of gyration of each protein using Flory's scaling law: $R_g = a \times N^{\nu}$, where $a = 0.3$ nm (73), N is the length of the protein, and $\nu = 0.34$. Scaling of $\nu = 0.34$ is expected for a polymer chain in a poor solvent and was confirmed for proteins by fitting >10,000 structures of folded proteins from the PDB (73) to the Flory expression above.

Data set of DBPs and MBPs with resolved structures

To perform structural analyses of DBPs and MBPs, we analyzed data sets of proteins with resolved structures, using a data set of proteins that form dimeric complexes as a control. The data sets of DBPs and of the control proteins were based on lists (74–76) that were further refined (34) such that 118 DBPs and 121 control proteins were included in the respective data sets. The list of MBPs was curated as follows: first, we searched the PDB for the Gene Ontology molecular function of "microtubule binding," for which we found 1007 protein chain entries. Only nontubulin structures with resolution <5 Å were retained, and the list was sorted in order of decreasing resolution. Next, we performed pairwise sequence alignment between all proteins in the list using the BioPython pairwise alignment module (77). Percent identity between two sequences was defined by dividing the number of matches by the length of the shorter sequence. Using the identity data, we kept the top structure (with the highest resolution) and eliminated chains with >70% sequence identity. This procedure was repeated with the second chain in the list and so on until the list was exhausted. The resulting set contained 78 MBPs (the full list of DBPs, MBPs, and dimers is in Table S2). All the proteins in the DBP, MBP, and dimeric protein data sets were analyzed for their charge densities and dipole moments (using the Protein Dipole Moment Server (78)).

RESULTS AND DISCUSSION

Proteins diffuse on DNA and MT with similar rates

To compare diffusion of proteins on DNA and on MTs, we first curated a data set containing experimentally studied DBPs and MBPs having known coefficients for diffusion on their respective biopolymer substrates. In Fig. 1, the diffusion coefficients, D, for a data set of 26 MBPs and 16 DBPs (see Table S1) are plotted vs. $1/R$, where R is the radius of the diffusing protein, estimated using Flory's scaling law for a polymer in a poor solvent (see Methods). The values of D for both DBPs and MBPs span approximately four orders of magnitude, between 0.001 and 1 $\mu m^2/s$. The dashed line in Fig. 1 is a liner fit of all the data points. The dashed line follows the Stokes-Einstein equation, which states $D = K_B T/6\pi\eta R$, where K_B is the Boltzmann constant, T is the temperature, η is viscosity, and R is the radius of the diffusing molecule. Energetic ruggedness for diffusion may contribute to deviation from a linear fit plot. The characteristic barrier for the energetic ruggedness of diffusion depends on the individual interactions of each DBP with DNA or each MBP with MT.

Electrostatic properties of diffusing proteins

Having observed that DBPs and MBPs diffuse at similar rates on DNA and MTs, respectively, we sought to compare their molecular mechanisms of diffusion on each substrate. For that purpose, we applied CG-MD simulations, which have previously been used to determine the molecular mechanism of protein diffusion on DNA (34,39,51–53) within protein-protein interfaces (50) and on MTs (54). In this study, we focused on three MBPs (PRC1, EB1, and Tau) and three DBPs (SAP1, HD, and Skn1), whose diffusion mechanisms were previously studied computationally (34,39) and experimentally (5,11).

The selected DBPs and MBPs have positively charged electrostatic surfaces (Fig. 2 *A*, *blue patches*; (79)) and similar dipole moment values (Fig. 2 *C*; (78)). However, the charge density of the DBPs is higher than the charge density of the MBPs (Fig. 2 *C*), as illustrated also by the darker shades of blue in the surface electrostatic map (Fig. 2 *A*). The higher content of positively charged residues in DBPs may lead to different diffusion mechanisms for DBPs and MBPs, as discussed below.

Electrostatic interactions dominate protein diffusion on DNA and MTs

To decipher the molecular determinants of protein diffusion, we studied the diffusion of the six selected DBPs and MBPs

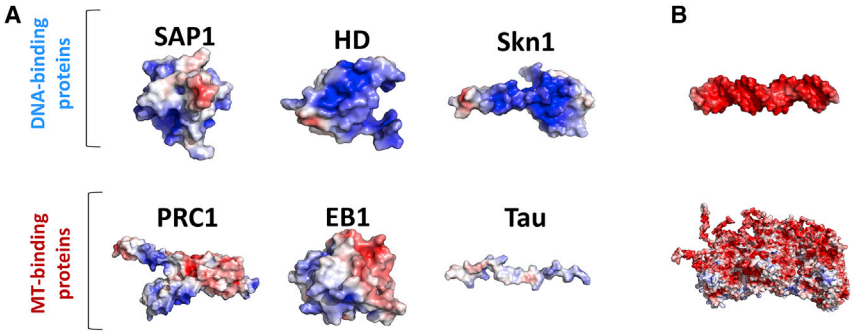

C

Protein	SAP1	HD	Skn1	PRC1	EB1	Tau
Dipole moment (Debye/res)	4.3	6.6	4.9	5.7	4.3	21.3
Net charge (per residue)	0.09	0.14	0.09	0.01	0.01	0.11
Positive charge (per residue)	0.16	0.24	0.23	0.20	0.13	0.18

FIGURE 2 Electrostatic properties of the simulated DBPs and MBPs. (*A*) Shown are cartoon representations of the three DBPs (SAP1, homeodomain (HD), and Skn1) and three MBPs (PRC1, EB1, and Tau) selected for the diffusion study. The electrostatic potential (79) is mapped on the surface of these proteins, with the positive and negative potential illustrated in blue and red, respectively. Both DBPs and MBPs have a large patch of positive potential, yet this is more pronounced for DBPs than for MBPs. (*B*). Electrostatic potentials for a DNA (*upper representation*) and an MT (*lower representation*) are shown, illustrating their negative electrostatic potential. (*C*). An electrostatic analysis of the six studied proteins is shown, highlighting their dipole moment, total net charge, and number of positive charges per residue. Although the dipole moment is similar for globular DBPs and MBPs, the DBPs have a higher net charge than the MBPs. Fig. 7 presents a similar analysis for 351 proteins. To see this figure in color, go online.

on both DNA and MTs to determine whether DBPs are likely to diffuse on MTs and MBPs are likely to diffuse on DNA simply because of the similarity in their electrostatic properties. The simulations revealed that all six proteins are attracted electrostatically to both DNA and MTs. Furthermore, the linear dependence of their mean-square displacement with time suggests that they diffuse along the main axis of the biopolymer (i.e., DNA or MTs). Fig. 3 shows the diffusion coefficients of these proteins on DNA (Fig. 3 *A*) and MTs (Fig. 3 *B*) for different salt concentrations (DBPs are shown in *blue* and MBPs in *red*). First, we note that the diffusion coefficients of the three DBPs on DNA and of the three MBPs on MTs have similar values, consistent with the experimental survey presented in Fig. 1. Specifically, the value of D for an HD diffusing on DNA (27) is ~2-fold higher than the value of D for EB1 and PRC1 on MTs, as was measured experimentally (5). Furthermore, MBPs diffuse faster than DBPs on both DNA and MTs. For all studied proteins, increasing salt concentration leads to an increase in the diffusion coefficient. However, MBPs diffuse faster than DBPs at any given salt concentration, and the increase in diffusion coefficient for MBPs is more pronounced than the increase for DBPs on all substrates, namely DNA (Fig. 3 *A*), MTs (Fig. 3 *B*), and MTs lacking disordered C-terminal tails (Fig. 3 *D*). However, although MBPs diffuse faster than DBPs on tailless MTs at low salt concentration (<0.03 M), this difference diminishes at higher salt concentrations. The contribution of tubulin C-terminal tails to the mechanism of protein diffusion on MTs will be discussed below.

One possible explanation for the faster diffusion of MBPs compared with DBPs is the observation that the charge density of the MBPs is lower than the charge density of the DBPs (Fig. 2). To test this possibility, we created 12 mutants of the DBP HD characterized by different combinations of three positive-to-negative residue substitutions, leading in all cases to a charge density similar to that of MBPs (positive charge per residue = 0.19 and net charge per residue = 0.01). We found that, although all the mutants tested had higher D than wild-type HD when diffusing on DNA (Fig. 3 *C*, mutants shown in *gray* and *black*; wild-type shown in *blue*), mutants with at least two mutated residues at the DNA recognition helix (Fig. 3 *C*, *black lines*) had higher D than the rest of the mutants at any given salt concentration (Fig. 3 *C*, *gray lines*). Moreover, mutating at least two positive residues at the DNA recognition helix led to loss of the characteristic rotation-translation-coupled diffusion along double-stranded DNA (Fig. 3 *C*, *inset*). Hence, we conclude that charge density alone does not fully explain the differences in D between MBPs and DBPs. The spatial organization of the charges within the structure of the diffusing protein is also important, as tested here for mutations in or out of the recognition helix of HD.

Furthermore, we tested whether there is a minimal number of positively charged residues at the recognition helix required to enable sliding of HD. For that purpose, we created an additional series of HD mutants in which the amount of positively charged residues at the recognition helix was varied and the rest of the residues of HD were neutralized: one mutant in which all six charged residues of the recognition helix remained charged, six mutants in which five residues remained charged, and 15 mutants in which four residues remained charged, considering all possible charge positions. We found that neutralizing two or more positive charges in any position of the recognition helix leads to the loss of the characteristic rotation-translation-coupled diffusion. Therefore, it appears that at least for the case of HD, a minimum of five positive charges at the recognition helix is sufficient, yet required, to slide along DNA in a rotation-translation coupled manner.

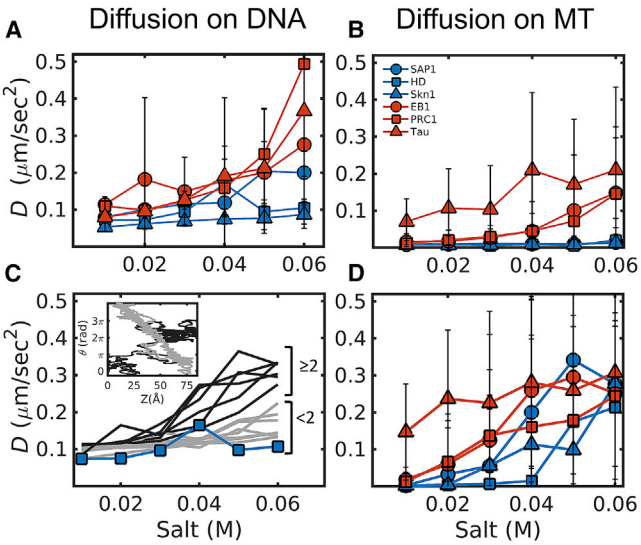

FIGURE 3 Properties of protein diffusion on DNA and MTs. (*A* and *B*) The diffusion coefficients, *D*, are given as a function of the salt concentration for the three selected DBPs (*blue*) and three selected MBPs (*red*) on DNA (*A*) and on MTs (*B*). The error bars represent the SD obtained from averaging the independent simulations (see Methods for details). *D* increases with the salt concentration for the diffusion of both types of proteins on both DNA and MTs. In addition, MBPs diffuse faster than DBPs on both DNA and MTs. (*C*) This is the same as (*A*) but for the mutants of DBP HD. Each line represents an HD mutant, in which three positive residues were replaced with three negative residues. The gray lines show mutants with <2 mutations in the recognition helix, and the black lines show mutants with ≥ 2 mutations in the recognition helix (residues 40–56 of HD). Inset: the coupling between the rotation (θ) around and translation (Z) along the DNA is shown for one HD mutant with <2 mutations in the recognition helix (*gray*) and one mutant with ≥ 2 mutations in the recognition helix (*black*). All the mutants have a positive charge per residue of 0.19 and a net charge per residue of 0.01. (*D*) This is the same as (*B*) but for the diffusion on MTs lacking C-terminal tails. Note that at low salt concentrations, MBPs (*red*) diffuse faster than DBPs (*blue*) and that this difference diminishes at higher salt concentrations. To see this figure in color, go online.

Diffusion of charged proteins along DNA or along MTs

To better understand the difference between MBPs and DBPs diffusing on DNA and MTs, we quantified the effect of the unique structural properties of DNA and MTs on diffusion. Fig. 4 *A* shows a projection of the COM of the DBP SAP1 (*blue*) and MBP PRC1 (*red*) as they diffuse on DNA, as simulated by CG-MD. Although SAP1 follows the DNA major groove, PRC1 does not. In a more quantitative analysis, Fig. 4 *B* shows the rotation angle between the diffusing proteins and the DNA as a function of translocation distance along the DNA axis (z). Whereas there is no clear relationship between rotation angle and translocation distance for any of the three MBPs (shown in *red*), the three DBPs demonstrate coupling between rotation and translocation along the DNA axis, as reflected by the slope of $2\pi/34 = 0.18$, which is characteristic of rotation-translation-coupled diffusion along double-stranded DNA. This indicates that all three DBPs diffuse along the DNA major groove, whereas the MBPs do not. Diffusion along the major DNA groove together with higher positive charge content can explain why DBPs diffuse more slowly than MBPs on DNA.

To complement this comparison, the diffusion of DBPs and MBPs was studied on an MT to examine why MBPs diffuse faster than DBPs on MTs, which do not have a major groove. Projections of the trajectories of the six studied proteins on an MT are shown in Fig. 5. Fig. 5 *A* shows that, whereas the DBP SAP1 is restricted to specific locations on the MT lattice, the MBP PRC1 samples a larger area of the MT lattice in the same accumulated simulation time. The heatmaps of the probability of finding the proteins at different locations on an MT lattice for all six proteins (Fig. 5 *B*) show that MBPs sample a larger fraction of the MT lattice than DBPs and that sidesteps across MT protofilaments, as discussed in detail elsewhere (54), also take place. It is possible that DBPs diffuse more slowly than MBPs on MTs and demonstrate a more restricted motion on MTs because they are more positively charged (Fig. 2).

MT tails modulate the diffusion of DBPs and MBPs on MTs

Although DNA and MTs are both very negatively charged (Fig. 2 *B*), they differ in that MTs are composed of two structural elements that are negatively charged: the globular parts of tubulin (MT body) and its C-terminal disordered tail (MT tail). A DBP or an MBP can, in principle, interact with both negatively charged elements, either in alternating or concomitant fashion. It is expected that DBP-MT interactions will be stronger than MBP-MT interactions even though the MT is not a natural substrate of DBPs simply because the DBPs have a greater net charge than MBPs.

To further explore the diffusion of DBPs and MBPs on MT, we followed the interactions of each protein with the two structural components of the MT. Heatmaps of the electrostatic interaction energies of the six studied proteins with MT body and MT tails are shown in Fig. 6. For all MBPs, the interaction energy between the protein and the MT body is >-5 kcal/mol, and the interaction energy between the protein and the MT tails is >-10 kcal/mol. The interaction of DBPs with the MT body and MT tails is ~2- to 3-fold stronger compared with the interaction of MBPs with these MT elements. Interestingly, although the DBP-to-MT-body interaction is ~2-fold stronger than the corresponding interaction for MBPs, the DBP-to-MT-tails interaction is ~3-fold stronger than the MBP-to-MT-tail interaction. The larger difference found in the strength of each protein's interaction with MT tails may indicate that whereas the MT body can interact with the diffusing proteins at a limited and defined interface, several disordered tubulin tails can interact with the protein simultaneously, resulting in a greater difference in interaction energy between DBPs and MBPs interacting with MT tails compared with MT bodies.

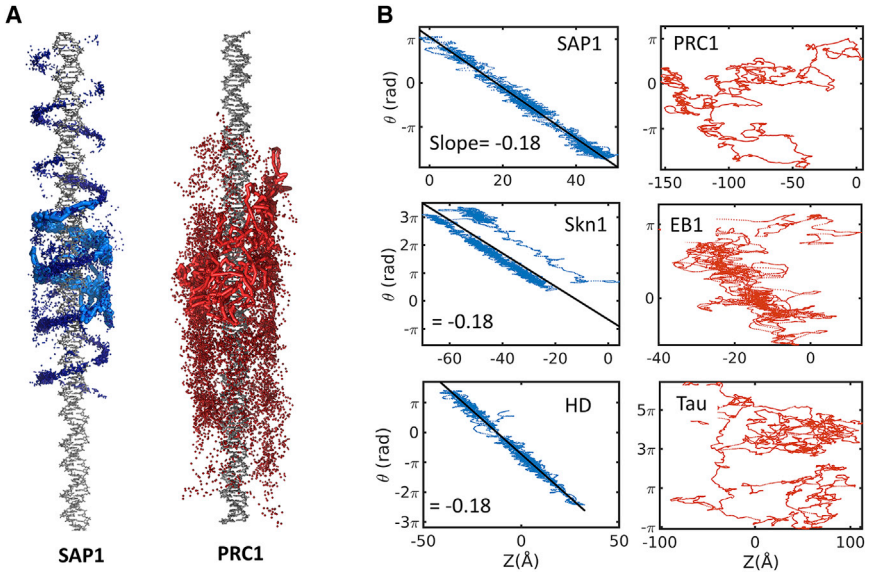

FIGURE 4 Structural properties of protein diffusion along DNA. (*A*) Shown is the projection of the location of the COM of the DBP SAP1 (*blue*) and the MBP PRC1 (*red*) during diffusion on DNA. Five trajectories are projected, and one of them is shown as a continuous thick line, demonstrating that SAP1 follows the DNA major groove and PRC1 does not. (*B*) Coupling between rotation and translation when diffusing along the DNA is examined by plotting the rotation angle (θ) versus the distance the protein traversed along the DNA axis (Z). The coupling between rotation and translation manifests as a straight-line relationship between θ and Z with a slope of $2\pi/34 = 0.18$, illustrating that DBPs diffuse helically on DNA (*left column*, *blue*); however, MBPs (*right column*, *red*) show no such coupling. To see this figure in color, go online.

Thus, the tubulin C-terminal tails, rather than the bodies, appear to be the more dominant contributor to the slow diffusion of DBPs on MTs. In addition, when we removed the C-terminal tails from the MTs, the difference in diffusion coefficients between the MBPs and DBPs at high salt concentrations diminished (Fig. 3 *D*).

Bioinformatic analysis of the electrostatic properties of DBPs and MBPs

Our results thus far suggest that for a protein to diffuse on a negatively charged biological polymer, be it DNA or an MT, the protein must have a combination of positively and negatively charged residues and, at least for the proteins used in this study, also a dipole moment. In addition, it appears that DBPs are more positively charged than MBPs and that the diffusion of DBPs and MBPs on DNA and MTs can be regulated by the unique structural features of each substrate (the major groove of DNA and the disordered C-terminal tails of tubulin). To test whether our observations can be generalized, we analyzed the electrostatic properties of 118 DBPs, 78 MBPs, and 121 dimers that served as a control set (see Methods for details on curation of the data sets). Indeed, the total charge density of DBPs (Fig. 7 *A*, *blue*) is higher than that of MBPs (Fig. 7 *A*, *red*) and the control set (Fig. 7 *A*, *gray*). In addition, the fraction of positively

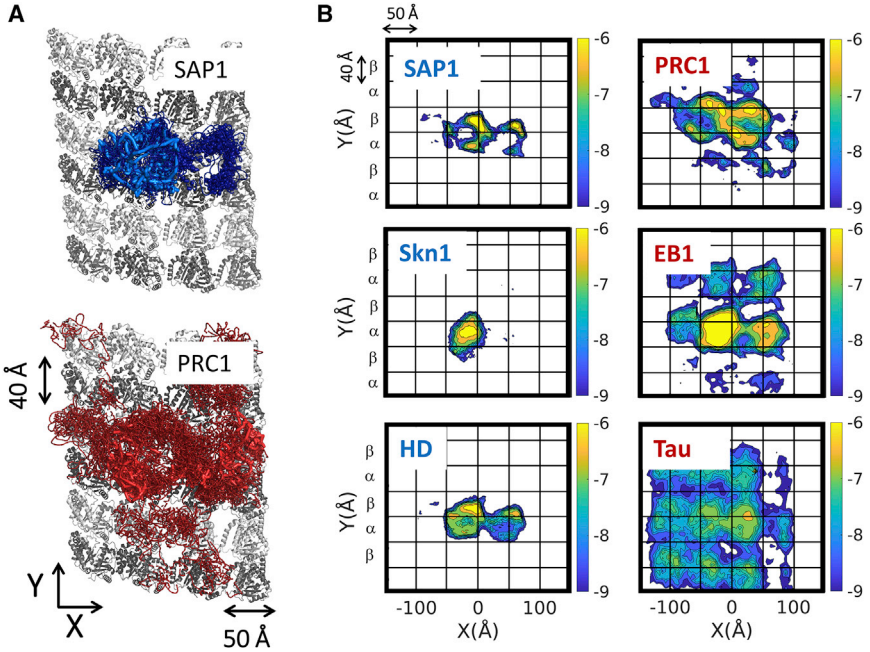

FIGURE 5 Structural properties of protein diffusion along MTs. (*A*) Shown is the projection of the location of the COM of the DBP SAP1 (*blue*) and MBP PRC1 (*red*) during diffusion on an MT lattice. 10 trajectories are projected on a slice of an MT lattice used in the CG simulations, and one trajectory is highlighted as a continuous thick line for each protein, demonstrating that PRC1 covers a larger fraction of the MT lattice than SAP1. (*B*) Shown are heatmaps of the probability of finding the diffusing protein at different locations on an MT lattice. The regions that are highly populated across the simulation time are colored yellow, and regions that are poorly populated are blue (see *color bar* on the *right*). The probability intensities are on a log scale and calculated for the COM of the diffusing proteins. DBPs sample a limited area of the MT lattice (*left panels*), whereas MBPs sample a larger fraction (*right panels*). The heatmaps shown here are from simulations at a salt concentration of 0.02 M. The grid lines reflect the lattice of α- and β-tubulins. To see this figure in color, go online.

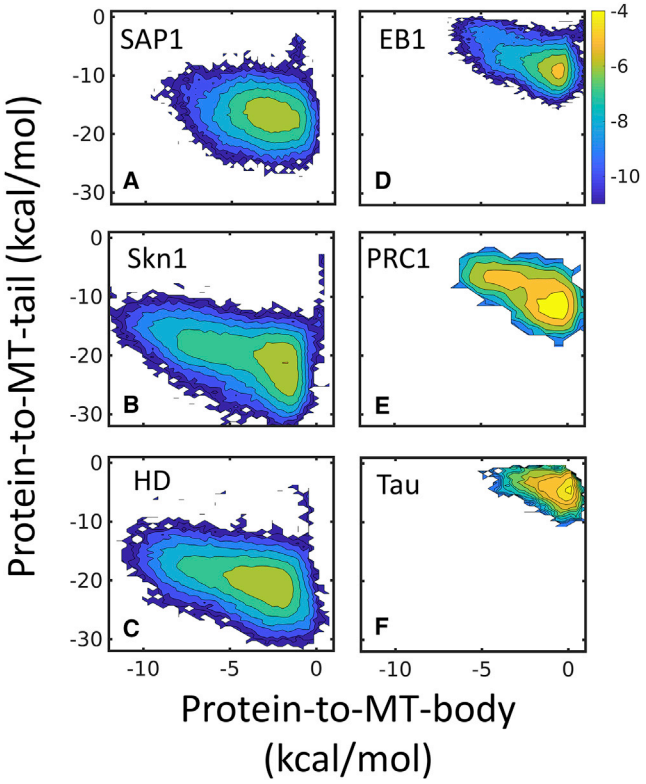

FIGURE 6 MT tails modulate the diffusion of DBPs and MBPs on MTs. The interactions of the DBPs or MBPs with the MT tails are shown in (*A*)–(*C*) and (*D*)–(*F*), respectively. Heatmaps of the interaction energy between the proteins and MT lattice, examined with respect to the MT tails (*y* axis) and MT body (*x* axis), show that DBPs interact more strongly than MBPs with MTs. The interaction energy between DBPs and the MT body is ~2-fold higher than that for MBPs, and the interaction energy between the DBPs and the MT tails is ~3-fold higher than that for MBPs. The analyzed trajectories were sampled at a salt concentration of 0.02 M. To see this figure in color, go online.

charged residues is greater in DBPs than in MBPs and the control set (Fig. 7 *B*). Similarly, DBPs have a larger dipole moment than MBPs and the control set. Hence, we conclude that our observations, namely that proteins that diffuse on DNA or MTs are more positively charged than proteins that do not and that DBPs have a larger dipole moment than MBPs, are general properties of DBPs and MBPs.

CONCLUSIONS

Protein diffusion on charged biopolymers, such as DNA and MTs, enables efficient scanning of DNA while proteins search for their cognate site and the localization of proteins to specific MT regions to perform their function, respectively. Because both DNA and MTs are negatively charged and proteins diffuse on the surfaces of DNA and MTs at similar rates, it is tempting to classify these two types of diffusion as sharing many similarities. However, a direct comparison between the two was lacking. Here, we addressed this question by quantifying the diffusion mechanisms of DBPs and MBPs on both their natural and unnatural substrates.

Using CG-MD modeling, we found that MBPs diffuse faster than DBPs on both DNA and MTs. The faster diffusion of MBPs was attributed to their lower net charge compared with DBPs. The lower charge density of MBPs compared with DBPs was confirmed by bioinformatic analysis of a larger data set of experimentally classified MBPs and DBPs. Although many positively charged proteins can diffuse on DNA, as demonstrated in this study, DBPs are unique in the sense that they can diffuse helically along the major groove, which may enable them to probe the DNA sequence and subsequently to bind specifically to their target sites. The ability of DBPs to slide along DNA while situated at the major groove is related to both electrostatic and structural complementarities. Reducing the electrostatic strength by increasing the salt concentration may shift diffusion on DNA from rotation-coupled translation along the major groove (also called sliding) to diffusion that lacks this coupling and is across major grooves (also called hopping). Mutating DBPs to reduce their charge density may result in diffusion via hopping, but this will strongly depend on the location of the mutations. Accordingly, charge

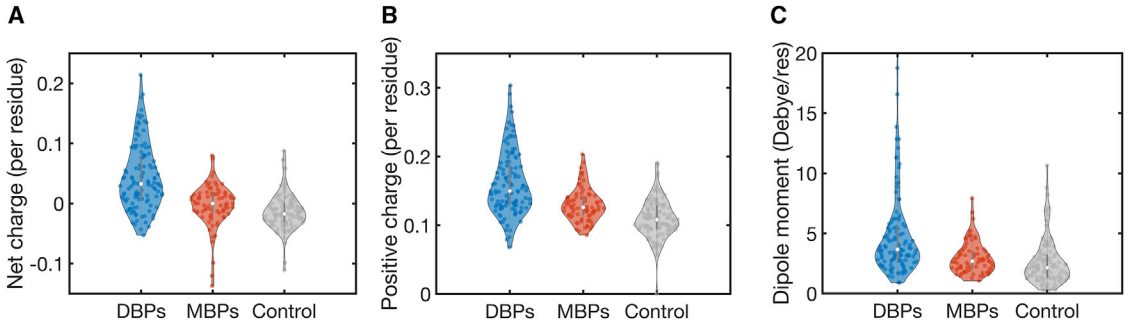

FIGURE 7 Electrostatic properties of DBPs and MBPs in large data sets. For 118 DBPs, 78 MBPs, and 121 homo- and heterodimeric proteins (control), the Protein Dipole Moment Server (78) was used to calculate the following: (*A*) net charge per residue, (*B*) positive charge per residue, and (*C*) dipole moment per residue. The mean dipole moments, the mean net charge, and the mean number of positive charges per residue are higher for the DBPs than for the MBPs. The mean number of positive charges is higher for MBPs compared with the control proteins. To see this figure in color, go online.

density is not the only parameter that governs the ability of DBPs to slide by rotation-coupled diffusion or that distinguishes between DBPs and MBPs. We note that several DBPs have been found to diffuse on DNA in a nonhelical fashion (i.e., hopping) (80,81).

MBPs, which have a lower charge density than DBPs, mostly perform hopping diffusion along DNA. The diffusion of MBPs along the MT is supported by the negatively charged disordered tails, which may compensate for the lower charge density of the MBPs and therefore increase their affinity to the MT. The interactions of MBPs with the tubulin tails can also explain why the experimentally observed diffusion rates of MBPs on MTs and of DBPs on DNA are similar, although MBPs have a lower charge density than DBPs. The observation that tubulin tails regulate protein diffusion on MTs is consistent with the regulatory role tubulin tails play in the interactions of several MBPs with MTs (56–60).

Although DBPs and MBPs are expected to usually diffuse on their natural substrates, in some cases they may encounter non-natural substrates. Proper cell division in eukaryotes requires recognition of the centromere by the DNA segregation machinery, connection between chromosomal DNA and spindle MTs, and force generation to move DNA to daughter cells (82). Therefore, during cell division, the MTs and DNA are in close proximity. Nonfunctional diffusion of DBPs on MTs and of MBPs on DNA may interfere with the functional interactions of DBPs and MBPs with their natural substrates. Hence, we speculate that the unique structural properties of MBPs, DBPs, MT, and DNA have co-evolved to assure proper cell division and to minimize the interference between the two types of proteins and their corresponding charged biopolymers.

SUPPORTING MATERIAL

Supporting Material can be found online at https://doi.org/10.1016/j.bpj.2020.05.004.

AUTHOR CONTRIBUTIONS

L.S.B. and Y.L. designed the research and wrote the manuscript. L.S.B. performed the research and analyzed the data.

REFERENCES

1. Hirokawa, N., and R. Takemura. 2005. Molecular motors and mechanisms of directional transport in neurons. *Nat. Rev. Neurosci.* 6:201–214.
2. Vale, R. D. 2003. The molecular motor toolbox for intracellular transport. *Cell.* 112:467–480.
3. Zhang, Z., and D. Thirumalai. 2012. Dissecting the kinematics of the kinesin step. *Structure.* 20:628–640.
4. Cooper, J. R., and L. Wordeman. 2009. The diffusive interaction of microtubule binding proteins. *Curr. Opin. Cell Biol.* 21:68–73.
5. Forth, S., K. C. Hsia, …, T. M. Kapoor. 2014. Asymmetric friction of nonmotor MAPs can lead to their directional motion in active microtubule networks. *Cell.* 157:420–432.
6. Westermann, S., H. W. Wang, …, G. Barnes. 2006. The Dam1 kinetochore ring complex moves processively on depolymerizing microtubule ends. *Nature.* 440:565–569.
7. Brouhard, G. J., J. H. Stear, …, A. A. Hyman. 2008. XMAP215 is a processive microtubule polymerase. *Cell.* 132:79–88.
8. Helenius, J., G. Brouhard, …, J. Howard. 2006. The depolymerizing kinesin MCAK uses lattice diffusion to rapidly target microtubule ends. *Nature.* 441:115–119.
9. Powers, A. F., A. D. Franck, …, C. L. Asbury. 2009. The Ndc80 kinetochore complex forms load-bearing attachments to dynamic microtubule tips via biased diffusion. *Cell.* 136:865–875.
10. Bieling, P., I. A. Telley, and T. Surrey. 2010. A minimal midzone protein module controls formation and length of antiparallel microtubule overlaps. *Cell.* 142:420–432.
11. Hinrichs, M. H., A. Jalal, …, T. Scholz. 2012. Tau protein diffuses along the microtubule lattice. *J. Biol. Chem.* 287:38559–38568.
12. Okada, Y. 1999. A processive single-headed motor: kinesin superfamily protein KIF1A. *Science.* 283:1152–1157.
13. Kwok, B. H., L. C. Kapitein, …, T. M. Kapoor. 2006. Allosteric inhibition of kinesin-5 modulates its processive directional motility. *Nat. Chem. Biol.* 2:480–485.
14. Hyeon, C., and J. N. Onuchic. 2007. Mechanical control of the directional stepping dynamics of the kinesin motor. *Proc. Natl. Acad. Sci. USA.* 104:17382–17387.
15. Zhang, Z., Y. Goldtzvik, and D. Thirumalai. 2017. Parsing the roles of neck-linker docking and tethered head diffusion in the stepping dynamics of kinesin. *Proc. Natl. Acad. Sci. USA.* 114:E9838–E9845.
16. Malaby, H. L., D. V. Lessard, …, J. Stumpff. 2019. KIF18A's neck linker permits navigation of microtubule-bound obstacles within the mitotic spindle. *Life Sci. Alliance.* 2:e201800169.
17. Bugiel, M., and E. Schäffer. 2018. Three-dimensional optical tweezers tracking resolves random sideward steps of the kinesin-8 Kip3. *Biophys. J.* 115:1993–2002.
18. Winter, R. B., and P. H. von Hippel. 1981. Diffusion-driven mechanisms of protein translocation on nucleic acids. 2. The *Escherichia coli* repressor–operator interaction: equilibrium measurements. *Biochemistry.* 20:6948–6960.
19. Halford, S. E. 2009. An end to 40 years of mistakes in DNA-protein association kinetics? *Biochem. Soc. Trans.* 37:343–348.
20. Halford, S. E., and J. F. Marko. 2004. How do site-specific DNA-binding proteins find their targets? *Nucleic Acids Res.* 32:3040–3052.
21. Kabata, H., O. Kurosawa, …, N. Shimamoto. 1993. Visualization of single molecules of RNA polymerase sliding along DNA. *Science.* 262:1561–1563.
22. Elf, J., G. W. Li, and X. S. Xie. 2007. Probing transcription factor dynamics at the single-molecule level in a living cell. *Science.* 316:1191–1194.
23. Tafvizi, A., F. Huang, …, A. M. van Oijen. 2011. A single-molecule characterization of p53 search on DNA. *Proc. Natl. Acad. Sci. USA.* 108:563–568.
24. Itoh, Y., A. Murata, …, K. Kamagata. 2018. Intrinsically disordered domain of tumor suppressor p53 facilitates target search by ultrafast transfer between different DNA strands. *Nucleic Acids Res.* 46:7261–7269.
25. Kamagata, K., A. Murata, …, S. Takahashi. 2017. Characterization of facilitated diffusion of tumor suppressor p53 along DNA using single-molecule fluorescence imaging. *J. Photochem. Photobiol. C Photochem. Rev.* 30:36–50.
26. Zandarashvili, L., D. Vuzman, …, J. Iwahara. 2012. Asymmetrical roles of zinc fingers in dynamic DNA-scanning process by the inducible transcription factor Egr-1. *Proc. Natl. Acad. Sci. USA.* 109:E1724–E1732.

27. Zandarashvili, L., A. Esadze, …, J. Iwahara. 2015. Balancing between affinity and speed in target DNA search by zinc-finger proteins via modulation of dynamic conformational ensemble. *Proc. Natl. Acad. Sci. USA.* 112:E5142–E5149.

28. Gorman, J., A. Chowdhury, …, E. C. Greene. 2007. Dynamic basis for one-dimensional DNA scanning by the mismatch repair complex Msh2-Msh6. *Mol. Cell.* 28:359–370.

29. Vuzman, D., A. Azia, and Y. Levy. 2010. Searching DNA via a "Monkey Bar" mechanism: the significance of disordered tails. *J. Mol. Biol.* 396:674–684.

30. Vuzman, D., M. Polonsky, and Y. Levy. 2010. Facilitated DNA search by multidomain transcription factors: cross talk via a flexible linker. *Biophys. J.* 99:1202–1211.

31. Kolomeisky, A. B. 2011. Physics of protein-DNA interactions: mechanisms of facilitated target search. *Phys. Chem. Chem. Phys.* 13:2088–2095.

32. Tafvizi, A., L. A. Mirny, and A. M. van Oijen. 2011. Dancing on DNA: kinetic aspects of search processes on DNA. *ChemPhysChem.* 12:1481–1489.

33. Slutsky, M., and L. A. Mirny. 2004. Kinetics of protein-DNA interaction: facilitated target location in sequence-dependent potential. *Biophys. J.* 87:4021–4035.

34. Marcovitz, A., and Y. Levy. 2011. Frustration in protein-DNA binding influences conformational switching and target search kinetics. *Proc. Natl. Acad. Sci. USA.* 108:17957–17962.

35. Marcovitz, A., and Y. Levy. 2013. Weak frustration regulates sliding and binding kinetics on rugged protein-DNA landscapes. *J. Phys. Chem. B.* 117:13005–13014.

36. Krepel, D., D. Gomez, …, Y. Levy. 2016. Mechanism of facilitated diffusion during a DNA search in crowded environments. *J. Phys. Chem. B.* 120:11113–11122.

37. Khazanov, N., A. Marcovitz, and Y. Levy. 2013. Asymmetric DNA-search dynamics by symmetric dimeric proteins. *Biochemistry.* 52:5335–5344.

38. Khazanov, N., and Y. Levy. 2011. Sliding of p53 along DNA can be modulated by its oligomeric state and by cross-talks between its constituent domains. *J. Mol. Biol.* 408:335–355.

39. Givaty, O., and Y. Levy. 2009. Protein sliding along DNA: dynamics and structural characterization. *J. Mol. Biol.* 385:1087–1097.

40. Terakawa, T., H. Kenzaki, and S. Takada. 2012. p53 searches on DNA by rotation-uncoupled sliding at C-terminal tails and restricted hopping of core domains. *J. Am. Chem. Soc.* 134:14555–14562.

41. Veksler, A., and A. B. Kolomeisky. 2013. Speed-selectivity paradox in the protein search for targets on DNA: is it real or not? *J. Phys. Chem. B.* 117:12695–12701.

42. Cézanne, L., A. Lopez, …, J. F. Tocanne. 1999. Organization and dynamics of the proteolipid complexes formed by annexin V and lipids in planar supported lipid bilayers. *Biochemistry.* 38:2779–2786.

43. Ziemba, B. P., J. D. Knight, and J. J. Falke. 2012. Assembly of membrane-bound protein complexes: detection and analysis by single molecule diffusion. *Biochemistry.* 51:1638–1647.

44. Vasquez, J. K., K. Chantranuvatana, …, J. D. Knight. 2014. Lateral diffusion of proteins on supported lipid bilayers: additive friction of synaptotagmin 7 C2A-C2B tandem domains. *Biochemistry.* 53:7904–7913.

45. Crosby, K. C., M. Postma, …, T. W. Gadella. 2013. Quantitative analysis of self-association and mobility of annexin A4 at the plasma membrane. *Biophys. J.* 104:1875–1885.

46. Ackmann, M., H. Wiech, and E. Mandelkow. 2000. Nonsaturable binding indicates clustering of tau on the microtubule surface in a paired helical filament-like conformation. *J. Biol. Chem.* 275:30335–30343.

47. Cochran, J. C. 2015. Kinesin motor enzymology: chemistry, structure, and physics of nanoscale molecular machines. *Biophys. Rev.* 7:269–299.

48. Subramanian, R., E. M. Wilson-Kubalek, …, T. M. Kapoor. 2010. Insights into antiparallel microtubule crosslinking by PRC1, a conserved nonmotor microtubule binding protein. *Cell.* 142:433–443.

49. Maurer, S. P., P. Bieling, …, T. Surrey. 2011. GTPgammaS microtubules mimic the growing microtubule end structure recognized by end-binding proteins (EBs). *Proc. Natl. Acad. Sci. USA.* 108:3988–3993.

50. Gomez, D., Y. Gavrilov, and Y. Levy. 2019. Sliding mechanism at a coiled-coil interface. *Biophys. J.* 116:1228–1238.

51. Mishra, G., and Y. Levy. 2015. Molecular determinants of the interactions between proteins and ssDNA. *Proc. Natl. Acad. Sci. USA.* 112:5033–5038.

52. Mishra, G., L. S. Bigman, and Y. Levy. 2020. ssDNA diffuses along replication protein A via a reptation mechanism. *Nucleic Acids Res.* 48:1701–1714.

53. Marcovitz, A., and Y. Levy. 2012. Sliding dynamics along DNA: a molecular erspective. *RSC Biomolecular Sciences.* 24:236–262.

54. Bigman, L. S., and Y. Levy. 2020. Tubulin tails and their modifications regulate protein diffusion on microtubules. *Proc. Natl. Acad. Sci. USA.* 117:8876–8883.

55. Bormuth, V., V. Varga, …, E. Schäffer. 2009. Protein friction limits diffusive and directed movements of kinesin motors on microtubules. *Science.* 325:870–873.

56. Serrano, L., J. Avila, and R. B. Maccioni. 1984. Controlled proteolysis of tubulin by subtilisin: localization of the site for MAP2 interaction. *Biochemistry.* 23:4675–4681.

57. Serrano, L., E. Montejo de Garcini, …, J. Avila. 1985. Localization of the tubulin binding site for tau protein. *Eur. J. Biochem.* 153:595–600.

58. Marya, P. K., Z. Syed, …, P. A. Eagles. 1994. Kinesin and tau bind to distinct sites on microtubules. *J. Cell Sci.* 107:339–344.

59. Wang, Z., and M. P. Sheetz. 2000. The C-terminus of tubulin increases cytoplasmic dynein and kinesin processivity. *Biophys. J.* 78:1955–1964.

60. Bailey, M. E., D. L. Sackett, and J. L. Ross. 2015. Katanin severing and binding microtubules are inhibited by tubulin carboxy tails. *Biophys. J.* 109:2546–2561.

61. Hyeon, C., and D. Thirumalai. 2005. Mechanical unfolding of RNA hairpins. *Proc. Natl. Acad. Sci. USA.* 102:6789–6794.

62. Clementi, C., H. Nymeyer, and J. N. Onuchic. 2000. Topological and energetic factors: what determines the structural details of the transition state ensemble and "en-route" intermediates for protein folding? An investigation for small globular proteins. *J. Mol. Biol.* 298:937–953.

63. Noel, J. K., P. C. Whitford, …, J. N. Onuchic. 2010. SMOG@ctbp: simplified deployment of structure-based models in GROMACS. *Nucleic Acids Res.* 38:W657–W661.

64. Noel, J. K., M. Levi, …, P. C. Whitford. 2016. SMOG 2: a versatile software package for generating structure-based models. *PLoS Comput. Biol.* 12:e1004794.

65. Azia, A., and Y. Levy. 2009. Nonnative electrostatic interactions can modulate protein folding: molecular dynamics with a grain of salt. *J. Mol. Biol.* 393:527–542.

66. Kissinger, C. R., B. S. Liu, …, C. O. Pabo. 1990. Crystal structure of an engrailed homeodomain-DNA complex at 2.8 A resolution: a framework for understanding homeodomain-DNA interactions. *Cell.* 63:579–590.

67. Mo, Y., B. Vaessen, …, R. Marmorstein. 1998. Structures of SAP-1 bound to DNA targets from the E74 and c-fos promoters: insights into DNA sequence discrimination by Ets proteins. *Mol. Cell.* 2:201–212.

68. Rupert, P. B., G. W. Daughdrill, …, B. W. Matthews. 1998. A new DNA-binding motif in the Skn-1 binding domain-DNA complex. *Nat. Struct. Biol.* 5:484–491.

69. Vemu, A., J. Atherton, …, A. Roll-Mecak. 2016. Structure and dynamics of single-isoform recombinant neuronal human tubulin. *J. Biol. Chem.* 291:12907–12915.

70. Hayashi, I., and M. Ikura. 2003. Crystal structure of the amino-terminal microtubule-binding domain of end-binding protein 1 (EB1). *J. Biol. Chem.* 278:36430–36434.

71. Kellogg, E. H., S. Howes, …, E. Nogales. 2016. Near-atomic cryo-EM structure of PRC1 bound to the microtubule. *Proc. Natl. Acad. Sci. USA.* 113:9430–9439.

72. Kellogg, E. H., N. M. A. Hejab, …, E. Nogales. 2018. Near-atomic model of microtubule-tau interactions. *Science.* 360:1242–1246.

73. Hofmann, H., A. Soranno, …, B. Schuler. 2012. Polymer scaling laws of unfolded and intrinsically disordered proteins quantified with single-molecule spectroscopy. *Proc. Natl. Acad. Sci. USA.* 109:16155–16160.

74. Szilágyi, A., and J. Skolnick. 2006. Efficient prediction of nucleic acid binding function from low-resolution protein structures. *J. Mol. Biol.* 358:922–933.

75. Bahadur, R. P., P. Chakrabarti, …, J. Janin. 2003. Dissecting subunit interfaces in homodimeric proteins. *Proteins.* 53:708–719.

76. Shaul, Y., and G. Schreiber. 2005. Exploring the charge space of protein-protein association: a proteomic study. *Proteins.* 60:341–352.

77. Cock, P. J., T. Antao, …, M. J. de Hoon. 2009. Biopython: freely available Python tools for computational molecular biology and bioinformatics. *Bioinformatics.* 25:1422–1423.

78. Felder, C. E., J. Prilusky, …, J. L. Sussman. 2007. A server and database for dipole moments of proteins. *Nucleic Acids Res.* 35:W512–W521.

79. Baker, N. A., D. Sept, …, J. A. McCammon. 2001. Electrostatics of nanosystems: application to microtubules and the ribosome. *Proc. Natl. Acad. Sci. USA.* 98:10037–10041.

80. Cuculis, L., Z. Abil, …, C. M. Schroeder. 2016. TALE proteins search DNA using a rotationally decoupled mechanism. *Nat. Chem. Biol.* 12:831–837.

81. Daitchman, D., H. M. Greenblatt, and Y. Levy. 2018. Diffusion of ring-shaped proteins along DNA: case study of sliding clamps. *Nucleic Acids Res.* 46:5935–5949.

82. Cheeseman, I. M. 2014. The kinetochore. *Cold Spring Harb. Perspect. Biol.* 6:a015826.

Biophysical Journal, Volume *118*

Supplemental Information

Protein Diffusion on Charged Biopolymers: DNA versus Microtubule

Lavi S. Bigman and Yaakov Levy

Table S1. List of diffusion coefficients for DNA and MT binding proteins.

Protein name	Rg (nm)	N	D1($\mu m^2/s$)	surface	Ref.
Nhp6	1.41	93	0.34	DNA	(1)
HU	1.39	90	0.49	DNA	(1)
Fis	1.44	98	0.16	DNA	(1)
PCNA	2.91	786	1.16	DNA	(2)
B clamp	2.84	732	0.01	DNA	(3)
P53 full	2.30	393	0.16	DNA	(4)
hOgg1	2.20	345	0.58	DNA	(5)
AVP-pVIc	1.88	215	2.20	DNA	(5)
MutY	2.25	369	0.17	DNA	(5)
MutM M74A	2.02	269	0.22	DNA	(5)
BamHI	1.87	213	0.57	DNA	(5)
1lacI	3.36	1196	0.05	DNA	(6)
EcoRV CyB3	1.96	245	1.20	DNA	(7)
MSH2-MSH6	4.14	2206	0.005	DNA	(8)
RNA polymerase	4.71	3233	0.01	DNA	(9)
Tale-cys3	3.19	1030	0.58	DNA	(10)
HoxD9	1.36	60	0.05	DNA	(11)
Tau	2.39	441	0.29	MT	(12–14)
EB1	2.51	506	0.02	MT	(15)
PRC1	2.59	555	0.04	MT	(15)
xmap215	4.02	2032	0.30	MT	(16)
NuMA	2.43	461	0.05	MT	(15)

p150 (basic domain)	2.56	540	0.0015	MT	(17)
p150	1.51	114	0.0017	MT	(17)
p150	3.43	1265	0.0014	MT	(17)
clip170	3.77	1676	0.0035	MT	(18)
coiled-col+Aurora-B	2.84	726	0.06	MT	(19)
Ndc80	3.87	1814	0.09	MT	(20)
ska1	2.92	788	0.23	MT	(20)
Clasp2	3.66	1532	0.33	MT	(20)
EB1	2.02	268	0.31	MT	(21)
NDC80	3.69	1576	0.17	MT	(22)
Mcak+GFP	3.12	963	0.38	MT	(23)
Qdot - Myosin Va	4.94	3710	0.26	MT	(24)
Myosin Va single headed	3.90	1855	0.36	MT	(23)
Kinesin 5 ADP (Eg5)	5.16	4224	0.0007	MT	(25)
Kinesin 5 ATP (Eg5)	5.16	4224	0.0008	MT	(25)
Yeast kinesin 8 (kip3)	3.21	1043	0.0043	MT	(26)
Dyenin , b IC subunit	5.30	4568	0.05	MT	(27)
Dyenin, outer arm	6.71	9136	0.01	MT	(27)
CENP-E	3.56	1422	0.07	MT	(28)
CENP-E tail	2.39	437	1.6	MT	(29)
POK2 (1-589)	3.75	1654	0.04	MT	(30)

Table S2. Electrostatic properties of DNA and MT binding proteins

PDB ID	Chain	Number of residues	Positive residues	Negative residues	Total charge	Dipole	Type
1bc8	C	93	15	6	9	405	DBP
1c9b	A	207	31	22	9	788	DBP
1cf7	B	82	14	10	4	279	DBP
1e3o	C	132	23	20	2	441	DBP
1efa	A	328	26	30	-3	1044	DBP
1f4k	A	115	23	17	6	412	DBP
1fjl	A	65	13	8	6	577	DBP
1hcr	A	52	10	3	7	285	DBP
1ign	A	189	31	30	2	594	DBP
1je8	A	63	14	7	8	305	DBP
1jt0	A	188	25	23	2	398	DBP
1k78	A	124	21	11	10	480	DBP
1lmb	3	87	10	12	-3	395	DBP
1mnm	C	77	16	7	9	350	DBP
1orn	A	214	36	26	10	929	DBP
1per	L	63	9	5	4	236	DBP
1pp7	U	114	18	13	4	420	DBP
1puf	A	77	21	7	14	479	DBP
1puf	B	73	15	8	7	828	DBP
1r71	A	114	18	23	-6	740	DBP
1r8d	A	109	16	18	-2	363	DBP
1rep	C	214	32	21	11	684	DBP
1rh6	B	52	11	7	4	245	DBP
1sax	A	120	21	18	3	1258	DBP
1sfu	A	70	12	6	6	379	DBP
1tc3	C	51	9	5	3	346	DBP
1tro	A	104	13	17	-4	641	DBP
2cgp	A	200	24	23	0	455	DBP
1l3l	A	447	67	60	7	907	DBP
1hlv	A	131	29	15	14	712	DBP
2irf	G	109	20	12	9	294	DBP
1dsz	A	75	14	6	7	385	DBP
1hwt	C	70	16	10	7	642	DBP
1mey	C	83	16	7	8	173	DBP
1ozj	A	126	23	15	8	782	DBP
1tsr	B	194	22	19	3	622	DBP
2drp	A	63	13	4	9	238	DBP

1a0a	A	63	10	5	5	810	DBP
1am9	A	80	19	8	11	629	DBP
1dh3	A	55	16	9	8	1372	DBP
1gd2	E	65	15	10	4	1591	DBP
1jnm	A	56	17	6	12	1734	DBP
1llm	C	87	18	13	5	1206	DBP
1mdy	A	68	18	8	10	1276	DBP
1nkp	B	83	17	11	5	1375	DBP
1nlw	A	79	19	10	9	851	DBP
1b3t	A	147	16	12	5	1241	DBP
1f44	A	316	47	37	10	1681	DBP
1flo	A	405	53	38	15	1284	DBP
1fzp	B	105	20	17	3	581	DBP
1h89	C	115	26	12	14	686	DBP
1jfi	B	135	18	20	-3	599	DBP
1jj4	A	74	11	5	6	215	DBP
1ku7	A	73	18	14	4	421	DBP
1kx5	B	102	25	7	18	1313	DBP
1kx5	C	128	26	9	17	1183	DBP
1kx5	D	122	28	9	19	1477	DBP
1mnm	A	85	15	9	6	960	DBP
1p7d	A	279	44	36	8	1109	DBP
1skn	P	74	17	10	7	369	DBP
1bdt	A	52	11	7	4	301	DBP
1c8c	A	64	16	8	8	152	DBP
1ecr	A	305	42	32	9	503	DBP
1h6f	A	184	31	19	11	452	DBP
1hjc	A	118	15	10	5	423	DBP
1mjo	A	104	16	19	-3	815	DBP
1owf	B	94	16	12	4	388	DBP
1p71	A	94	17	13	4	324	DBP
1qna	A	182	29	15	14	892	DBP
1a3q	A	285	45	33	12	878	DBP
1e3m	A	765	90	105	-15	1736	DBP
1j3e	A	115	12	12	-1	643	DBP
1jb7	A	460	62	53	9	420	DBP
1jb7	B	216	29	26	3	196	DBP
1jey	A	493	72	69	3	1953	DBP
1mnn	A	290	40	36	4	1819	DBP
1p7h	L	286	38	31	7	795	DBP
1pt3	A	128	28	17	12	466	DBP
1a31	A	457	84	69	15	774	DBP

1a73	A	162	11	9	2	582	DBP
1bl0	A	116	17	14	2	593	DBP
1cez	A	862	104	107	-3	2074	DBP
1d02	A	197	25	27	-2	373	DBP
1dc1	A	310	40	45	-4	904	DBP
1dct	A	324	44	34	10	1011	DBP
1dfm	A	218	28	32	-3	885	DBP
1diz	A	282	28	26	2	526	DBP
1emh	A	223	26	21	5	573	DBP
1bhm	B	208	28	32	-4	579	DBP
1ewn	A	200	26	22	4	356	DBP
1fiu	A	286	30	34	-4	483	DBP
1g38	A	393	53	50	3	1120	DBP
1g9z	A	152	22	17	5	306	DBP
1i3j	A	96	19	7	13	929	DBP
1i6j	A	256	27	24	3	764	DBP
1iaw	A	304	39	40	-2	1035	DBP
1jx4	A	335	62	51	11	799	DBP
1k3x	A	253	30	27	2	563	DBP
1kc6	A	249	31	35	-4	668	DBP
1m3q	A	314	29	31	-2	568	DBP
1m5r	A	351	49	43	6	827	DBP
1mus	A	458	69	52	17	1452	DBP
1nk4	A	580	77	89	-12	1583	DBP
1p8k	Z	252	39	28	11	708	DBP
1qum	A	279	26	38	-12	409	DBP
1r2z	A	273	40	31	8	975	DBP
1rrq	A	344	43	54	-11	918	DBP
1rzt	A	327	43	35	8	1045	DBP
1sl1	A	678	84	101	-17	2976	DBP
1sx5	A	244	34	30	4	427	DBP
1t3n	A	388	48	45	3	1530	DBP
1vas	A	137	22	16	6	493	DBP
2dnj	A	253	21	29	-8	349	DBP
3pvi	A	156	18	20	-2	633	DBP
6mht	A	327	40	39	1	1019	DBP
1dew	A	279	35	34	1	747	DBP
1oup	A	210	27	20	7	985	DBP
2p5o	A	831	108	116	-6	1763	DBP
6hyo	A	131	20	19	0	547	MBP
2qjz	A	117	17	14	2	613	MBP
5lxx	A	477	46	63	-17	758	MBP

1f9v	A	313	31	35	-4	727	MBP
2qfa	A	137	22	25	-3	852	MBP
5lzn	A	111	14	11	4	252	MBP
4kml	A	109	10	14	-4	273	MBP
4o59	O	332	36	33	3	602	MBP
5d94	A	119	18	16	3	614	MBP
2xhi	A	316	30	30	1	666	MBP
2zfi	A	329	40	41	-1	1514	MBP
5fmu	A	131	22	16	6	483	MBP
1ry6	A	319	46	42	4	470	MBP
2o0a	A	270	31	38	-6	387	MBP
2vvg	A	308	38	35	2	881	MBP
4a14	A	296	29	41	-13	1437	MBP
4ggf	C	108	13	20	-6	336	MBP
3mmy	A	354	35	35	0	617	MBP
3zcw	A	321	39	42	-3	1039	MBP
1fzq	A	176	20	23	-3	560	MBP
4b91	A	474	49	56	-7	980	MBP
3zfd	A	340	45	40	4	712	MBP
3nrx	A	123	25	24	1	565	MBP
6mq7	A	244	31	33	-2	616	MBP
1bg2	A	323	39	43	-5	968	MBP
1eo6	A	116	18	17	1	249	MBP
3b6u	A	323	44	39	4	622	MBP
5wde	A	320	34	43	-8	1206	MBP
5fmt	A	134	16	14	2	170	MBP
2of3	A	266	38	35	3	582	MBP
2qjx	A	115	19	15	4	380	MBP
3dc4	A	291	25	26	-1	828	MBP
4au8	A	276	37	32	5	964	MBP
6ctn	A	326	52	47	5	1152	MBP
3wx8	A	153	21	17	4	302	MBP
4g3a	A	220	28	32	-3	757	MBP
3nwn	A	308	32	35	-2	663	MBP
4ja7	A	466	58	62	-4	2114	MBP
4c9y	A	120	23	14	9	210	MBP
2heh	A	324	47	37	10	936	MBP
6mq5	A	227	30	27	2	584	MBP
2ct9	A	185	25	35	-10	723	MBP
3cob	A	355	48	44	5	566	MBP
3lre	A	289	35	30	5	836	MBP
6jzc	A	251	35	22	13	803	MBP

6nje	A	297	37	32	5	435	MBP
1ft1	A	315	40	50	-10	333	MBP
5wdh	A	298	28	30	-3	661	MBP
1goj	A	354	42	38	4	938	MBP
5azh	A	127	16	18	-3	600	MBP
6nwp	A	75	13	7	6	507	MBP
2ggm	A	142	25	38	-14	510	MBP
3t0q	A	304	34	34	0	779	MBP
3u06	A	359	37	48	-11	850	MBP
6b5c	A	293	43	47	-4	771	MBP
4gkp	A	229	28	30	-1	361	MBP
1t5c	A	322	42	36	5	548	MBP
3fwb	A	153	18	39	-21	735	MBP
4xa3	A	142	20	28	-9	469	MBP
5x3e	A	375	43	48	-5	678	MBP
5c46	F	175	22	23	-2	385	MBP
4bn2	A	326	37	32	6	891	MBP
5gsz	A	306	33	40	-7	604	MBP
4rfx	A	100	14	26	-12	481	MBP
2owm	A	328	38	45	-6	1462	MBP
5an9	J	250	46	40	6	922	MBP
5wc1	A	262	34	37	-3	850	MBP
4aj5	K	108	19	18	1	857	MBP
6gvw	A	312	33	35	-2	719	MBP
6b0i	K	368	52	41	11	603	MBP
6h3c	A	255	34	29	5	699	MBP
5nd4	C	337	42	31	11	598	MBP
5mlv	A	344	41	40	0	910	MBP
5mm4	K	382	44	45	-1	652	MBP
5mjs	D	121	17	16	1	335	MBP
5m5c	C	118	16	12	4	357	MBP
1ycs	A	191	22	19	3	593	heterodimer
1ycs	B	193	11	35	-25	755	heterodimer
1a4y	A	460	40	62	-22	1362	heterodimer
1a4y	B	123	20	10	10	319	heterodimer
1qbk	B	856	79	121	-41	973	heterodimer
1qbk	C	187	27	18	9	1301	heterodimer
1am4	A	199	15	20	-6	763	heterodimer
1am4	D	174	19	21	-3	399	heterodimer
1emv	A	83	7	15	-8	370	heterodimer
1emv	B	131	26	21	5	291	heterodimer
1fin	A	298	37	33	4	142	heterodimer

1fin	B	260	26	30	-4	738	heterodimer
1d09	A	310	30	35	-5	954	heterodimer
1d09	B	153	19	19	0	427	heterodimer
1wq1	R	166	19	27	-8	300	heterodimer
1wq1	G	320	34	40	-6	764	heterodimer
1fss	A	532	49	58	-9	1847	heterodimer
1fss	B	61	9	5	4	212	heterodimer
1ef1	A	289	45	40	5	1925	heterodimer
1ef1	C	87	19	19	0	221	heterodimer
1f60	A	440	61	54	7	366	heterodimer
1f60	B	90	7	19	-13	583	heterodimer
1itb	A	153	18	19	-1	507	heterodimer
1itb	B	310	36	39	-3	1952	heterodimer
1ai8	H	249	37	30	7	419	heterodimer
1ai8	I	9	0	4	-5	112	heterodimer
2pcf	A	99	6	15	-9	292	heterodimer
2pcf	B	250	27	28	-1	806	heterodimer
1bml	A	250	26	23	3	349	heterodimer
1bml	C	318	37	51	-14	457	heterodimer
1frv	A	262	22	28	-6	244	heterodimer
1frv	B	530	60	60	0	819	heterodimer
2pcb	A	294	33	44	-11	844	heterodimer
2pcb	B	104	21	12	9	242	heterodimer
1tba	A	67	5	14	-10	288	heterodimer
1tba	B	180	27	15	12	855	heterodimer
12as	A	327	33	47	-14	787	homodimer
1a3c	A	166	23	27	-4	603	homodimer
1a4i	A	285	30	36	-6	407	homodimer
1a4u	A	254	25	24	1	608	homodimer
1aa7	A	158	18	16	2	457	homodimer
1ad3	A	446	48	54	-6	637	homodimer
1ade	A	431	50	60	-10	742	homodimer
1af5	A	126	15	12	4	257	homodimer
1afw	A	390	38	41	-2	915	homodimer
1ajs	A	412	45	43	2	523	homodimer
1amk	A	250	25	23	2	86	homodimer
1aor	A	605	73	84	-11	843	homodimer
1aq6	A	245	23	30	-7	190	homodimer
1auo	A	218	15	24	-9	231	homodimer
1b3a	A	67	10	5	4	408	homodimer
1b5e	A	241	28	33	-5	136	homodimer
1b67	A	68	13	12	1	232	homodimer

1b8a	A	438	60	76	-16	3101	homodimer
1b8j	A	448	41	52	-11	279	homodimer
1bam	A	200	26	31	-5	794	homodimer
1bbh	A	131	14	18	-4	454	homodimer
1bd0	A	381	42	45	-3	663	homodimer
1bif	A	432	54	64	-10	127	homodimer
1biq	A	339	33	48	-15	167	homodimer
1bis	A	146	16	16	0	321	homodimer
1bjw	A	381	44	50	-6	1000	homodimer
1bkp	A	278	31	40	-9	768	homodimer
1bmd	A	327	36	42	-6	485	homodimer
1brw	A	433	52	57	-5	935	homodimer
1bsl	A	323	28	44	-16	105	homodimer
1bsr	A	124	17	9	9	406	homodimer
1buo	A	121	8	16	-8	843	homodimer
1bxg	A	349	24	41	-17	979	homodimer
1bxk	A	341	32	43	-11	293	homodimer
1cdc	A	96	13	13	0	312	homodimer
1cg2	A	389	48	51	-3	138	homodimer
1chm	A	401	41	55	-14	1158	homodimer
1cmb	A	104	15	19	-4	676	homodimer
1cnz	A	363	37	47	-10	656	homodimer
1coz	A	126	19	23	-4	133	homodimer
1csh	A	435	41	41	0	734	homodimer
1ctt	A	294	21	30	-9	313	homodimer
1cvu	A	552	56	59	-3	996	homodimer
1czj	A	110	11	15	-4	503	homodimer
1daa	A	277	36	41	-5	479	homodimer
1dor	A	311	27	37	-10	433	homodimer
1dpg	A	485	54	76	-22	303	homodimer
1dqs	A	381	47	44	2	495	homodimer
1dxg	A	36	3	7	-4	86	homodimer
1e98	A	210	32	29	3	264	homodimer
1ebh	A	436	51	56	-5	539	homodimer
1f13	A	722	81	95	-12	1676	homodimer
1fip	A	73	11	7	3	521	homodimer
1fro	A	176	23	28	-5	395	homodimer
1gvp	A	87	10	7	3	178	homodimer
1hhp	A	99	10	8	1	401	homodimer
1hjr	A	158	15	12	3	515	homodimer
1hss	A	111	11	10	1	292	homodimer
1hxp	A	340	33	42	-9	798	homodimer

1icw	A	69	13	8	4	297	homodimer
1imb	A	273	27	34	-5	326	homodimer
1isa	A	192	13	19	-6	212	homodimer
1ivy	A	452	38	43	-5	537	homodimer
1jhg	A	101	13	16	-3	688	homodimer
1jsg	A	111	13	18	-5	210	homodimer
1kba	A	66	5	4	2	259	homodimer
1kpf	A	111	12	13	-2	450	homodimer
1lyn	A	125	22	11	11	357	homodimer
1m6p	A	146	19	19	-1	186	homodimer
1mkb	A	171	20	21	-1	360	homodimer
1mor	A	366	34	47	-13	424	homodimer
1nox	A	200	27	23	3	297	homodimer
1nse	A	416	40	44	-4	1275	homodimer
1nsy	A	271	36	46	-10	207	homodimer
1oac	A	719	74	95	-21	1067	homodimer
1opy	A	123	9	16	-7	284	homodimer
1pgt	A	210	20	23	-3	169	homodimer
1pre	A	449	40	47	-8	1242	homodimer
1qfh	A	212	20	29	-8	1204	homodimer
1qhi	A	304	24	27	-2	314	homodimer
1qr2	A	230	22	26	-4	349	homodimer
1r2f	A	283	23	35	-12	370	homodimer
1reg	A	122	21	18	3	371	homodimer
1rfb	A	119	18	19	-1	211	homodimer
1rpo	A	61	7	13	-6	651	homodimer
1ses	A	421	58	62	-4	1125	homodimer
1slt	A	130	13	16	-3	214	homodimer
1smn	A	241	24	24	0	584	homodimer
1smt	A	98	9	9	-1	670	homodimer
1sox	A	463	46	59	-13	1219	homodimer
1tc1	A	175	24	25	-1	456	homodimer
1tox	A	515	51	65	-12	1661	homodimer
1trk	A	678	65	69	-4	319	homodimer
1uby	A	348	44	51	-7	678	homodimer
1utg	A	70	9	10	-1	300	homodimer
1vfr	A	217	24	32	-8	378	homodimer
1vok	A	192	30	16	14	898	homodimer
1wtl	A	108	8	8	-1	235	homodimer
1xso	A	150	12	19	-7	242	homodimer
2arc	A	161	14	16	-3	359	homodimer
2ccy	A	127	17	15	2	270	homodimer

2hdh	A	286	37	35	3	815	homodimer
2ilk	A	155	22	21	1	692	homodimer
2lig	A	157	11	14	-3	209	homodimer
2mcg	A	215	17	18	-1	510	homodimer
2nac	A	374	38	48	-10	282	homodimer
2ohx	A	374	42	38	4	725	homodimer
2spc	A	107	15	20	-5	880	homodimer
2sqc	A	623	69	82	-13	1279	homodimer
2tct	A	198	21	26	-5	783	homodimer
2tgi	A	112	11	10	1	485	homodimer
3dap	A	320	30	45	-15	425	homodimer
3grs	A	461	50	49	1	1027	homodimer
3sdh	A	145	19	15	4	446	homodimer
3ssi	A	108	6	10	-4	439	homodimer
4cha	A	11	0	0	0	97	homodimer
4kbp	A	424	47	43	5	1959	homodimer
5csm	A	250	37	39	-2	280	homodimer
5rub	A	436	43	48	-6	836	homodimer
8prk	A	282	35	43	-8	382	homodimer
9wga	A	170	10	9	2	186	homodimer

References:

1. Kamagata, K., E. Mano, K. Ouchi, S. Kanbayashi, and R.C. Johnson. 2018. High Free-Energy Barrier of 1D Diffusion Along DNA by Architectural DNA-Binding Proteins. J. Mol. Biol. 430: 655–667.
2. Kochaniak, A.B., S. Habuchi, J.J. Loparo, D.J. Chang, K.A. Cimprich, J.C. Walter, and A.M. van Oijen. 2009. Proliferating cell nuclear antigen uses two distinct modes to move along DNA. J. Biol. Chem. 284: 17700–17710.
3. Laurence, T.A., Y. Kwon, A. Johnson, C.W. Hollars, M. O'Donnell, J.A. Camarero, and D. Barsky. 2008. Motion of a DNA sliding clamp observed by single molecule fluorescence spectroscopy. J. Biol. Chem. 283: 22895–22906.
4. Tafvizi, A., F. Huang, A.R. Fersht, L.A. Mirny, and A.M. van Oijen. 2011. A single-molecule characterization of p53 search on DNA. Proc. Natl. Acad. Sci. U. S. A. 108: 563–568.
5. Blainey, P.C., G. Luo, S.C. Kou, W.F. Mangel, G.L. Verdine, B. Bagchi, and X.S. Xie. 2009. Nonspecifically bound proteins spin while diffusing along DNA. Nat. Struct. Mol. Biol. 16: 1224–1229.
6. Elf, J., G.W. Li, and X.S. Xie. 2007. Probing transcription factor dynamics at the single-molecule level in a living cell. Science (80-.). 316: 1191–1194.
7. Dikić, J., C. Menges, S. Clarke, M. Kokkinidis, A. Pingoud, W. Wende, and P. Desbiolles. 2012. The rotation-coupled sliding of EcoRV. Nucleic Acids Res. 40: 4064–4070.
8. Gorman, J., A. Chowdhury, J.A. Surtees, J. Shimada, D.R. Reichman, E. Alani, and E.C. Greene. 2007. Dynamic Basis for One-Dimensional DNA Scanning by the Mismatch Repair Complex Msh2-Msh6. Mol. Cell. 28: 359–370.
9. Harada, Y., T. Funatsu, K. Murakami, Y. Nonoyama, A. Ishihama, and T. Yanagida. 1999. Single-molecule imaging of RNA polymerase-DNA interactions in real time. Biophys. J. 76: 709–715.
10. Cuculis, L., Z. Abil, H. Zhao, and C.M. Schroeder. 2016. TALE proteins search DNA using a rotationally decoupled mechanism. Nat. Chem. Biol. 12: 831–837.
11. Sahu, D., and J. Iwahara. 2017. Discrete-State Kinetics Model for NMR-Based Analysis of Protein Translocation on DNA at Equilibrium. J. Phys. Chem. B. 121: 9548–9556.
12. Hinrichs, M.H., A. Jalal, B. Brenner, E. Mandelkow, S. Kumar, and T. Scholz. 2012.

Tau protein diffuses along the microtubule lattice. J. Biol. Chem. 287: 38559–38568.

13. Mcvicker, D.P., G.J. Hoeprich, A.R. Thompson, and C.L. Berger. 2014. Tau interconverts between diffusive and stable populations on the microtubule surface in an isoform and lattice specific manner. Cytoskeleton. 71: 184–194.
14. Scholz, T., and E. Mandelkow. 2014. Transport and diffusion of Tau protein in neurons. Cell. Mol. Life Sci. 71: 3139–3150.
15. Forth, S., K.C. Hsia, Y. Shimamoto, and T.M. Kapoor. 2014. Asymmetric friction of nonmotor MAPs can lead to their directional motion in active microtubule networks. Cell. 157: 420–432.
16. Brouhard, G.J., J.H. Stear, T.L. Noetzel, J. Al-Bassam, K. Kinoshita, S.C. Harrison, J. Howard, and A.A. Hyman. 2008. XMAP215 Is a Processive Microtubule Polymerase. Cell. 132: 79–88.
17. Culver-Hanlon, T.L., S.A. Lex, A.D. Stephens, N.J. Quintyne, and S.J. King. 2006. A microtubule-binding domain in dynactin increases dynein processivity by skating along microtubules. Nat. Cell Biol. 8: 264–270.
18. Dixit, R., B. Barnett, J.E. Lazarus, M. Tokito, Y.E. Goldman, and E.L.F. Holzbaur. 2009. Microtubule plus-end tracking by CLIP-170 requires EB1. Proc. Natl. Acad. Sci. 106: 492–497.
19. Noujaim, M., S. Bechstedt, M. Wieczorek, and G.J. Brouhard. 2014. Microtubules accelerate the kinase activity of Aurora-B by a reduction in dimensionality. PLoS One. 9: e86786.
20. Chakraborty, M., E. V. Tarasovetc, A. V. Zaytsev, M. Godzi, A.C. Figueiredo, F.I. Ataullakhanov, and E.L. Grishchuk. 2019. Microtubule end conversion mediated by motors and diffusing proteins with no intrinsic microtubule end-binding activity. Nat. Commun. 10.
21. Lopez, B.J., and M.T. Valentine. 2016. The +TIP coordinating protein EB1 is highly dynamic and diffusive on microtubules, sensitive to GTP analog, ionic strength, and EB1 concentration. Cytoskeleton. 73: 23–34.
22. Powers, A.F., A.D. Franck, D.R. Gestaut, J. Cooper, B. Gracyzk, R.R. Wei, L. Wordeman, T.N. Davis, and C.L. Asbury. 2009. The Ndc80 Kinetochore Complex Forms Load-Bearing Attachments to Dynamic Microtubule Tips via Biased Diffusion. Cell. 136: 865–875.
23. Helenius, J., G. Brouhard, Y. Kalaidzidis, S. Diez, and J. Howard. 2006. The depolymerizing kinesin MCAK uses lattice diffusion to rapidly target microtubule ends.

Nature. 441: 115–119.

24. Ali, M.Y., E.B. Krementsova, G.G. Kennedy, R. Mahaffy, T.D. Pollard, K.M. Trybus, and D.M. Warshaw. 2007. Myosin Va maneuvers through actin intersections and diffuses along microtubules. Proc. Natl. Acad. Sci. 104: 4332–4336.
25. Kwok, B.H., L.C. Kapitein, J.H. Kim, E.J.G. Peterman, C.F. Schmidt, and T.M. Kapoor. 2006. Allosteric inhibition of kinesin-5 modulates its processive directional motility. Nat. Chem. Biol. 2: 480–485.
26. Bormuth, V., V. Varga, J. Howard, and E. Schäffer. 2009. Protein friction limits diffusive and directed movements of kinesin motors on microtubules. Science (80-.). 325: 870–873.
27. Vale, R.D., D.R. Soll, and I.R. Gibbons. 1989. One-dimensional diffusion of microtubules bound to flagellar dynein. Cell. 59: 915–925.
28. Kim, Y., J.E. Heuser, C.M. Waterman, and D.W. Cleveland. 2008. CENP-E combines a slow, processive motor and a flexible coiled coil to produce an essential motile kinetochore tether. J. Cell Biol. 181: 411–419.
29. Gudimchuk, N., B. Vitre, Y. Kim, A. Kiyatkin, D.W. Cleveland, F.I. Ataullakhanov, and E.L. Grishchuk. 2013. Kinetochore kinesin CENP-E is a processive bi-directional tracker of dynamic microtubule tips. Nat. Cell Biol. 15: 1079–1088.
30. Chugh, M., M. Reißner, M. Bugiel, E. Lipka, A. Herrmann, B. Roy, S. Müller, and E. Schäffer. 2018. Phragmoplast Orienting Kinesin 2 Is a Weak Motor Switching between Processive and Diffusive Modes. Biophys. J. 115: 375–385.